1

Alignment and orientation of molecules in matrices

Toni Kiljunen[1] and Burkhard Schmidt[2] and Nikolaus Schwentner[3]

[1] University of Jyväskylä, Department of Chemistry, P.O. Box 35, FIN–40014 Finland, toni.kiljunen@jyu.fi
[2] Freie Universität, Institute of Mathematics II, Arnimallee 6, D–14195 Berlin, Germany, burkhard@math.fu-berlin.de
[3] Freie Universität, Institute of Physics, Arnimallee 22, D–14195 Berlin, Germany, schwentner@physik.fu-berlin.de

1.1 Introduction

In the previous sections of this chapter the molecular photodynamics of matrix-isolated di-halogen molecules upon electronic excitation has been investigated. In all those studies the initial alignment or orientation of the guest molecule with respect to the crystallographic axes of the host lattice has been fixed. Indeed, this assumption is valid for larger chromophores occupying two (or more) adjacent substitutional sites. In that case, the guest rotational degrees of freedom are essentially frozen which allows, e. g., for the construction of low-dimensional models of (coupled) host–guest systems [1, 2]. In contrast, smaller molecules occupying mono–substitutional sites are — to a certain extent — exhibiting rotational motion. The degree of hindering depends strongly on the nature of the guest–host interaction which shall be loosely termed "crystal field" throughout the following text. With increasing field strength, the rotational states undergo a gradual transition from free rotor states via hindered rotor states to librational states. In the latter case, the rotational motion is strongly frustrated and the molecular axes undergo angular vibrations about certain crystallographic directions. In general, the crystal field is determined by a subtle interplay of attractive and repulsive interaction of the guest molecule with the surrounding rare gas atoms. For example, the energetically preferred axes of the HF@Ar and HCl@Ar systems are along the $\langle 111 \rangle$ direction with the guest molecules pointing towards the triatomic windows formed by the nearest neighbors in the face–centered cubic rare gas crystal. [3, 4]. In contrast, the ClF@Ar system favors the $\langle 100 \rangle$ direction, i. e. tetra-atomic windows, while in a Kr matrix the ClF molecules are preferentially oriented directly towards the nearest neighbors located on the $\langle 110 \rangle$ axes [5, 6].

Obviously, the different directionality of rotational states of matrix-isolated molecules can have enormous implications on their photochemical properties: A preferred orientation of the guest molecules towards nearest neighbors typically results in strong reflections from the solvent cage eventually leading to recombination of the photofragments. In contrast, a molecular orientation towards windows of the first solvation shell is more likely to lead to cage exit and permanent separation of the photofragments. Hence, a promising approach to control the yield of matrix photodissociation proceeds via controlling the alignment and/or orientation of matrix-isolated molecule [7]. Similar approaches for librational control of photochemistry have already been suggested for diatomic molecules embedded in rare gas clusters [8–11]. It is the purpose of this section to review the state of the art in the manipulation of rotational degrees of freedom of matrix-embedded molecules, utilizing both time-independent and time-dependent methods, as documented in a recent series of articles [5, 6, 12–14]

For gas phase molecules the manipulation of rotational degrees of freedom has already reached a relatively mature state, for a review see Ref. [15]. Because the interaction of external fields with molecular dipole moments is limited to molecules with strong dipoles and requires very strong static fields [16, 17], efficient approaches to molecular alignment and orientation are nowadays based on the nonresonant interaction of intense laser fields with induced dipoles due to anisotropic molecular polarizabilities [18–22]. The use of linear, circular, and elliptic polarization allows to fix one, two, or all three axes of molecular rotation with respect to the laboratory frame. The corresponding molecular quantum states are termed pendular states which are defined as superpositions of field-free rotor states where the molecular axis librates about the polarization direction of the field [18, 23, 24]. In contrast to most other control mechanisms discussed in this book, light–induced alignment is usually achieved using nonresonant fields. This makes the control very robust with respect to variations of the laser pulse parameters, and in most cases excellent quantitative agreement between theory and experiment is found. Due to the cylindrical symmetry of the molecule–field interaction, pendular states occur in pairs of different parity which are connected by tunnelling through the barrier provided by the $\cos^2$-shaped light-induced potential. This gives rise to a straight–forward approach of achieving molecular orientation: By applying a static field, oriented molecular states can be formed as superpositions of tunnelling pairs of pendular states [25, 26]. The necessary electrostatic field strengths may be several orders of magnitude lower than in the pendular orientation approach using static fields alone [16, 17]. The concept of orientation by combined fields has been experimentally verified for molecules both in gas phase [27, 28] and in small rare gas clusters [29, 30].

In time-dependent molecular alignment, the rotational dynamics induced by pulsed light sources can be characterized by the following two limits: The adiabatic limit can be approached by using light pulses which are long compared to the rotational period of the molecule. In that case, however, align-

ment can only be achieved while the field is turned on [15]. Field-free alignment can be found in the nonadiabatic case, where the molecules interact with pulses much shorter than the rotational time scale. This leads to the formation of rotational wave packet states that can be considered as coherent superpositions of field-free states and the post-pulse evolution is dominated by corresponding quantum beats and rotational revivals [31]. Further "squeezing" of the rotational densities can be achieved by tailored "pulse trains", i. e., by suitable sequences of pulses [32–36].

In the present work we want to elucidate the question in how far the results on the control of gas phase alignment and orientation can be transferred to the situation of matrix-isolated molecules. Based on the above concept of matrix-induced librational states, the following control objectives can be identified: (1) In a *cooperative* case, the targeted direction of alignment already coincides with the energetically preferred axes, i. e., the minima of the (internal) crystal field. In that case, the interaction with (external) laser fields can be utilized to further narrow the rotational distributions, possibly beyond the gas phase case. (2) In more challenging, *competitive* cases the control objective is to enforce the alignment of rotational states towards directions which correspond to saddles, or even maxima, of the crystal field [12]. To this end, the rotational densities will have to be turned by the external alignment field against the effect of the internal crystal field. Furthermore, the question is whether there exists a matrix analog to the gas phase mechanism of achieving additional "head vs. tail" orientation by means of combined field.

1.2 Model and interactions

In the following we shall restrict ourselves to the case of a linear molecule in an electronically non-degenerate $^1\Sigma$ state occupying a mono-substitutional site in an fcc lattice, e. g., hydrogen halides or other small diatomic molecules in solid rare gases [37]. Furthermore, we shall neglect any coupling of the rotational to translational [38], vibrational [39, 40], or electronic [41] degrees of freedom of the guest molecule. While the latter two assumptions can be justified by the rather low temperatures considered in the present work, a non-coinciding center of mass and center of interaction could lead to rotation-translation coupling. However, the resulting eccentric rotational motion can be accounted for by appropriate down-scaling of the rotational constant B [42,43]. Moreover, interaction between the external fields and the surrounding matrix can be neglected for rare gases as long as the field intensities are below damage thresholds of the respective rare gas crystal. Then the resulting Hamiltonian for the rotational motion of the diatomic guest molecule can be written as

$$\hat{H}/B = (\hat{\mathbf{J}}/\hbar)^2 + \hat{V}_\kappa + \hat{V}_\alpha + \hat{V}_\mu \,, \tag{1.1}$$

where $\hat{\mathbf{J}}$ is the angular momentum operator of the embedded molecule and the remaining three terms stand for the interaction with the matrix ($\hat{V}_\kappa$) as well as with (nonresonant) laser fields ($\hat{V}_\alpha$) and electrostatic fields ($\hat{V}_\mu$).

Assuming a perfectly ordered fcc lattice environment, the guest–host interaction ("crystal field") is expanded in symmetry adapted spherical harmonics (SASHs) of the totally symmetric representation (A_{1g}) of the octahedral point group (O_h) [44]. Usually only the two lowest SASHs (V_4, V_6) are considered

$$V_\kappa(\theta,\phi;\kappa) = \kappa\left[K_4 V_4(\theta,\phi) + K_6 V_6(\theta,\phi)\right] , \tag{1.2}$$

where κ is a (dimensionless) scaling parameter. Building on the seminal studies of librational states in V_4 potentials [45], the effect of different shapes of hindering potentials was discussed in the literature [46,47]. In the present work the parameters $K_4 = -52\sqrt{\pi}/(11\sqrt{21})$ and $K_6 = 16\sqrt{\pi}/(11\sqrt{26})$ are chosen such that the minima are along the six $\langle 100\rangle$ directions with $V_{\min}/\kappa = -1$, the saddles are along the twelve $\langle 110\rangle$ directions with $V_{\rm sad}/\kappa = 0$, and the maxima are along the eight $\langle 111\rangle$ directions with $V_{\max}/\kappa = 10/9$ [13, 14], see left panel of Fig. 1.1. This potential is very similar in shape to that obtained for a simplified DIM model of ClF@Ar [5, 6]. According to the target directions relative to the extrema of the rotational potential, the case of alignment/orientation along $\langle 100\rangle$ (minima) shall be termed cooperative, while the case of $\langle 110\rangle$ (saddles) or $\langle 111\rangle$ (maxima) shall be referred to as competitive in the following [12].

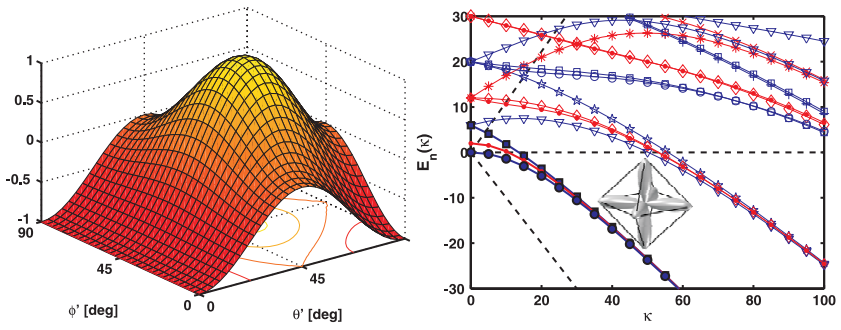

Fig. 1.1. Left: Octahedral "crystal field" model potential $V_\kappa(\theta,\phi)/\kappa$ of Eq. (1.2) with minima at the $\langle 100\rangle$ crystallographic axes ($\theta = 0$), saddle points at the $\langle 110\rangle$ axes ($\theta = \pi/2$, $\phi = \pi/4$), and maxima at the $\langle 111\rangle$ axes ($\theta = \cos^{-1} 1/\sqrt{3}$, $\phi = \pi/4$). Right: Corresponding energy spectrum versus strength parameter of the potential. The dashed lines show the maxima, saddles, and minima of the potential energy surface. The various symbols denote different irreducible representations of the O_h point group. Ground state rotational density for $\kappa = 25$ is inserted in the octahedron. Reproduced with permission from [13]

The nonresonant interaction of a laser field $\mathcal{E}_\mathrm{L}$ with the induced dipole moment of the molecule leads to an effective, light–induced potential of the form

$$V_\alpha(\theta;\Delta\omega) = -(\Delta\omega\cos^2\theta + \omega_\perp)\,, \tag{1.3}$$

where the (dimensionless) interaction strength is related to the laser field and (parallel and perpendicular) components of the molecular polarizability through $\omega_{\parallel,\perp} = \mathcal{E}_\mathrm{L}^2\alpha_{\parallel,\perp}/(4B)$ with $\Delta\omega = \omega_\parallel - \omega_\perp$ and where θ is defined as the angle between the field direction and the molecular axis [25]. Note that polarization along fourfold $\langle 100\rangle$, threefold $\langle 111\rangle$, and twofold $\langle 110\rangle$ rotational axes reduces the octahedral (O_h) point group of the librational states to the D_{4h}, D_{3d}, and D_{2h} subgroups, respectively. Finally, the interaction of an electrostatic field $\mathcal{E}_\mathrm{S}$ with the dipole moment μ of the molecule is given by

$$V_\mu(\theta;\omega) = -\omega\cos\theta \tag{1.4}$$

with the dimensionless parameter $\omega = \mu\mathcal{E}_\mathrm{S}/B$. Due to the absence of inversion symmetry, the respective point groups are further reduced to C_{4v}, C_{3v}, and C_{2v}. The conversions of dimensionless static field, laser intensity, temperature, $\gamma = k_BT/B$, and time, $\tau = 2Bt/h$, into practical units are given by

$$\begin{aligned}
\mathcal{E}_S[\mathrm{kV\,cm^{-1}}] &= \frac{B[\mathrm{cm^{-1}}]}{0.0168\,\mu[\mathrm{D}]}\omega \\
\mathcal{I}_0[\mathrm{W\,cm^{-2}}] &= \frac{B[\mathrm{cm^{-1}}]}{2.11\times10^{-11}\Delta\alpha[10^{-30}\mathrm{m^3}]}\Delta\omega \\
T[\mathrm{K}] &= 1.44B[\mathrm{cm^{-1}}]\gamma \\
t[\mathrm{ps}] &= \frac{16.68}{B[\mathrm{cm^{-1}}]}\tau
\end{aligned} \tag{1.5}$$

1.3 From free rotors to librational states

The main distinction between the manipulation of external degrees of freedom of gas phase and matrix-isolated molecules is that in the latter case the rotational motion of molecules is governed by the crystal field, V_κ, describing the interaction with the surroundings. Upon increasing its strength, the rotational states are gradually changing from free rotor states to hindered states, until, finally, the limit of librational states is approached, i. e., angular oscillations about preferred crystallographic axes [48–50]. In Fig. 1.1 these three regimes can be approximately identified from their energies with respect to minima, saddles and maxima of the model potential given in Eq. (1.2). Starting from the free rotor states $|JM\rangle$ for $\kappa = 0$ with energies $E/B = J(J+1)$ and degeneracies $g = 2J+1$, essentially free rotation is still observed for $E > V_\mathrm{max}$. The regime of $V_\mathrm{max} > E > V_\mathrm{sad}$ is characterized by hindered rotor states with

degeneracies $g = 1, 2, 3$ in case of A, E, T cubic symmetry, respectively. For $V_{\rm sad} > E > V_{\rm min}$, the energy level scheme is dominated by librational manifolds of states which can be labelled by quantum numbers $n = 0, 1, \ldots$ with corresponding degeneracies $g = 6(n + 1)$ for rotational densities along $\langle 100 \rangle$ directionality.

Another aspect is the dependence of the energy levels on the crystal field parameter: Beyond certain thresholds for κ, all energy levels tend to decrease with increasing κ ("low-field seeking" states) and form manifolds of librational states. As can be seen in the right panel of Fig. 1.1, for the model potential [Eq. (1.2)] chosen here, the formation of the first and second manifold is found at $\kappa \approx 20$ and $\kappa \approx 60$, respectively. In the following we shall restrict ourselves to a fixed field strength $\kappa = 25$ where the potential wells are deep enough to support directional states as shown in the inserts in the right panel of Fig. 1.1. Here the first multiplet has already formed and the typical multi-scale nature of librational states of matrix-isolated molecules already becomes apparent: While the crystal field splitting — as well as the zero point energy — is of the order of $10B$, the nearly degenerate ground state is comprised of a set of states (here A_{1g}, T_{1u}, and E_g) exhibiting tunnel splittings below $1B$. Accordingly, the fields used for alignment/orientation are termed as strong if they can achieve notable mixing of states belonging to different multiplets, while weak fields can only mix states inside a single set. Note that in the first case rotational densities are driven above potential energy saddles or barriers, while they can tunnel in the second case.

1.4 From librational to pendular states

In the following we discuss optically-dressed, pendular states for the combined action of the matrix- and light-induced potentials, $V_\kappa + V_\alpha$ for constant crystal field, $\kappa = 25$. The resulting energy levels, $E_n(\Delta\omega)$, for cooperative $\langle 100 \rangle$ alignment are shown in the upper left part of Fig. 1.2. We neglect the angle–independent part of V_α in Eq. (1.3) by setting $\omega_\perp = 0$. First of all, the degeneracies of the E and T symmetry librational states are lifted as the field is switched on ($\Delta\omega > 0$) due to the reduction of the symmetry point group from O_h to D_{4h}, see the group theoretical considerations in [13]. Secondly, we note that there are two classes of states: While one set of energy levels is essentially field–insensitive, the remaining states are high-field seeking, i. e., they gain energy for increasing laser intensity $\Delta\omega$. This different behavior is due to the directionality of the wave functions with their lobes pointing either perpendicular or parallel to the field. While the first ones essentially remain unchanged, the rotational densities of the latter ones become gradually more squeezed along the direction of the external field. Due to the non-crossing rule for states of equal symmetry, this leads to avoided crossings.

The degree of alignment of pendular states is usually measured in terms of the alignment cosine, $\langle \cos^2 \theta \rangle$. This expectation value vanishes for a per-

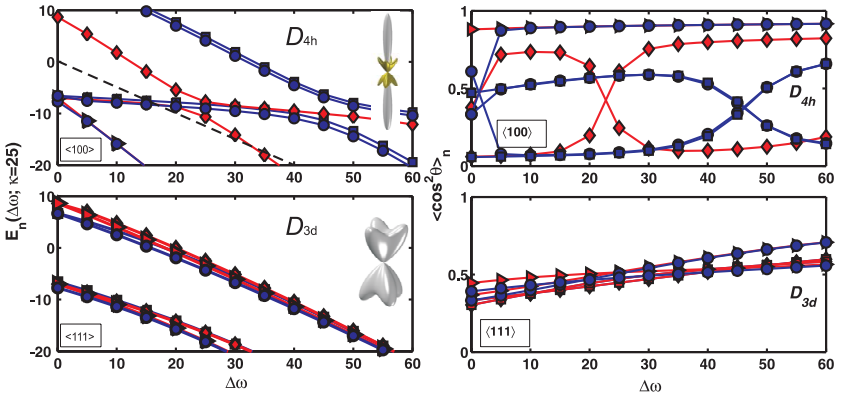

Fig. 1.2. Energy spectrum (left panel) and alignment cosine (right panel) versus strength of interaction $\Delta\omega$ of guest molecule with external laser field [Eq. (1.3)] for fixed internal field, $\kappa = 25$. Upper and lower figures correspond to cooperative $\langle 100 \rangle$ and competitive $\langle 111 \rangle$ polarization of the laser field, respectively.

pendicular state, it is one third for an isotropic state, and it approaches unity for the limit of infinitely narrow wave functions. It is related to (the slopes of) the energy levels by virtue of the Hellmann–Feynman theorem

$$\langle \cos^2 \theta \rangle_n = -\frac{\partial E_n}{\partial(\Delta\omega)} \,. \tag{1.6}$$

This is visible in the upper right panel of Fig. 1.2, where the perpendicular states with $\langle \cos^2 \theta \rangle < 0.1$ can be readily distinguished from the parallel states with $\langle \cos^2 \theta \rangle > 0.9$, where the alignment cosine of the (parallel) ground state exceeds that obtained for the gas phase case [25]. Moreover, the pattern of avoided crossings of the energy levels is clearly reproduced for the alignment cosine. The sudden increase of alignment hints to an abrupt change of the character of the states rather than the smooth narrowing observed for the parallel states not involved in crossings. A qualitatively similar picture emerges for the competitive case of $\langle 110 \rangle$ alignment (not shown in the figure), but with reduced maximal alignment, $\langle \cos^2 \theta \rangle < 0.75$. The case of $\langle 111 \rangle$ alignment, however, is distinctly different, see lower part of Fig. 1.2: All states are high-field seeking, and there are no clear crossings visible. For vanishing crystal field, $\Delta\omega = 0$, the alignment is near the isotropic value of $1/3$ because the librational states under investigation exhibit notable rotational density neither parallel nor perpendicular to the threefold $\langle 111 \rangle$ target. For the range of interactions considered here ($\Delta\omega \leq 60$), the alignment cosine $\langle \cos^2 \theta \rangle$ does not exceed a value of 0.7.

In Ref. [13] we also discuss the degree of alignment for two thermal ensembles $\gamma = 1$ and $\gamma = 10$ in detail. For these temperatures the thermal energies are insufficient or sufficient to overcome rotational barriers, respectively.

While equal weighting of pendular states would always result in an isotropic distribution, significant thermally averaged alignment is observed due to the higher Boltzmann weights of the energetically lower states usually bearing higher alignment. Moreover, the averaged results are insensitive to the dramatic changes of the components at avoided crossings, because parallel and perpendicular states merely change their role.

In the cooperative case, the parallel directions of crystal field minima and laser polarization lead to more effective alignment than in the gas phase: For the lower temperature, $\gamma = 1$, high degrees of alignment (> 0.9) can be achieved for fields one order of magnitude weaker than in the gas phase case. The enhancement is still significant for the higher temperature, $\gamma = 10$. In the competitive cases, where alignment along saddles or maxima of the crystal field is strived for, the maximal, thermally averaged alignment remains below the corresponding gas phase values. For the range of (dimensionless) laser intensities studied here ($\Delta\omega \leq 60$), only moderate values around 0.6–0.7 can be achieved for $\kappa = 25$, whereas the averaged alignment does not exceed the isotropic value notably for stronger matrix field, $\kappa = 60$.

In the case of a homo-nuclear diatomic molecule, the above-described techniques for alignment of the molecular axis relative to the crystallographic axes completely suffice to fix the rotational degrees of freedom. For a hetero-nuclear molecule, however, additional "head vs. tail" orientation may be desired in the control of photochemical events. In principle, this can be achieved by interaction V_μ of an electrostatic field with the molecular dipole moment, see Eq. (1.4). In practice, however, this "brute force" orientation is restricted to rather high values of the (dimensionless) interaction parameter ω [16, 17]. A more elegant approach to orientation of gas phase molecules circumvents this problem by utilizing combined laser and static field, $V_\alpha + V_\mu$. As mentioned in the Introduction, the laser field serves to create (degenerate) g/u pairs of states, which can be split by rather weak static fields. In close analogy, we have devised a similar approach to orientation of molecules trapped in octahedral fields that builds on a combination of crystal and electrostatic fields, $V_\kappa + V_\mu$ [13]. As shown in the right panel of Fig. 1.1, the crystal field gives rise to the formation of a quasi-degenerate set of librational states which are connected to each other by two-dimensional tunnelling. If the matrix-induced field is sufficiently strong, then the tunnelling splittings of energy levels become sufficiently small, such that they can be efficiently manipulated by rather weak electrostatic fields.

Pendular, oriented states resulting from the combined action of the matrix-induced (crystal) field and electrostatic (orientation) fields, $V_\kappa + V_\mu$ are shown in Fig. 1.3, again for constant crystal field, $\kappa = 25$. The resulting energy levels, $E_n(\omega)$ are shown in the upper and lower left part of the figure for cooperative $\langle 100 \rangle$ and competitive $\langle 111 \rangle$ orientation. As in the case of laser-induced alignment, most of the degeneracies are lifted due to the lowering of the O_h to the C_{nv} point groups due to the $\cos\theta$ type interaction V_μ. In addition to field–insensitive (perpendicular) and high-field seeking (parallel)

states, we observe also the existence of low-field seeking states with orientation anti-parallel to the external static field. Again, the non-crossing rule describes the behavior at the intersections: States transforming according to equal or unequal irreducible representations of the respective C_{nv} point groups are undergoing avoided or true intersections, respectively. Of particular interest are the avoided crossings of parallel and anti-parallel states observed both for the cooperative and competitive case. These events correspond to sudden 180 degree flips of oriented rotational wave functions. The slope of the energy plots is connected through a Hellmann–Feynman relation [similar to Eq. (1.6)] for the orientation cosine $\langle \cos\theta \rangle$ used to quantify orientation effects. The right hand side of Fig. 1.3 shows our results: While the qualitative picture is similar, it is obvious that the achieved maximal degree of orientation is higher in the cooperative case ($\langle \cos\theta \rangle \approx 0.95$) than in the competitive case ($\langle \cos\theta \rangle \approx 0.65$). When including the effect of thermal averaging, higher orientation than for gas phase molecules is found in the former case while the opposite is true for the latter case.

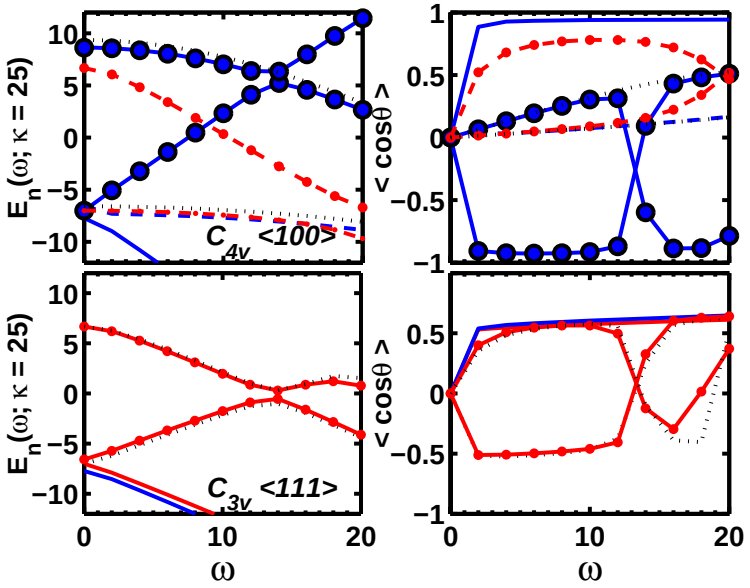

Fig. 1.3. Energy spectrum (left panel) and orientation cosine (right panel) versus strength of interaction ω of guest molecule with external static field [Eq. (1.4)] for fixed internal field, $\kappa = 25$. Upper and lower figures correspond to cooperative $\langle 100 \rangle$ and competitive $\langle 111 \rangle$ direction of the static field, respectively.

Another interesting aspect is the dependence of alignment and orientation on the strength of the crystal field: As discussed in more detail in [13], very *weak* laser or static fields are necessary to achieve very high degrees of alignment or orientation, respectively, for the cooperative case. For instance, for $\kappa \approx 100$, (dimensionless) interaction parameters $(\Delta\omega, \omega)$ of the order of 0.1 are sufficient to achieve near unity alignment or orientation if single pendular state are considered. However, as discussed above, *strong* fields with interaction parameters $(\Delta\omega, \omega)$ of the order of 10-100 are needed to achieve high alignment/orientation for a thermal ensemble. This is particularly true for the competitive cases, where strong fields are required even at rather low temperatures.

1.5 From analysis to control of rotational dynamics in matrices

So far, we have discussed the manipulation of rotational degrees of freedom of matrix-isolated molecules in terms of time-independent wave functions and their expectation values, i. e., alignment and orientation cosines. In realistic experiments, however, the respective control targets are achieved by means of pulsed light sources. As well as most other light-induced processes discussed in this book, the time-dependent picture of alignment/orientation of molecules in matrices can be categorized with respect to the adiabatic and nonadiabatic limit, depending whether the employed pulses are long or short with respect to the inherent time scales of the systems under investigation.

First, let us consider the nonadiabatic case: The use of ultra-short laser pulses generally renders the system in a wave-packet state, i. e., a coherent superposition of eigenstates of the quantum system under investigation. Upon time-evolution of a wave packet, each of the comprising states exhibits phase oscillations with its own frequency $E_n B/\hbar$. Hence, any time-dependent observable (expectation value) of a superposition is dominated by beating patterns $(E_n - E_m)B/\hbar$. In particular, recurrences occur, where two or more of the underlying oscillations are in phase. To illustrate this principle, we first consider the rotational motion of gas phase molecules. The thermally averaged alignment signal, $\langle\langle\cos^2\theta\rangle\rangle(\tau)$, obtained for interaction of a linear molecule with an intense laser pulse ($\Delta\omega = 100$) and for low temperature ($\gamma = 1$) is shown in the top left panel of Fig. 1.4. The very short, Gaussian-shaped pulse (FWHM: $\sigma = 0.032$) creates a rotationally broad wave packet, and strongly nonadiabatic dynamics is observed with complex temporal oscillation patterns of the post-pulse alignment [51–53]. Note that on average the alignment cosine stays above the isotropic value 1/3. Signatures of recurrences are clearly visible: After $\tau = 1$ the wave packet is again spatially aligned due to complete phase matching of the rotational components and the initial alignment peak is regained. In addition, a free molecule exhibits

fractional revivals, e. g. at $\tau = 1/2$, where the rotational density is delocalized in a plane perpendicular to the polarization of the field. This dip in the alignment signal (anti-alignment) [54] is surrounded by two peaks with high parallel alignment. In general, the simple energy level scheme of a free rotor leads to the observation of the (fractional) revival intervals. Obviously, the corresponding energy differences can be extracted from the complex beating pattern by virtue of a Fourier transform: The power spectrum in the upper right of Fig. 1.4 shows progression within gerade parity states ($J = 0, 2 \cdots 8$) by distinct peaks ($4J + 6$) at 6, 14, 22, and 30, and the peak at $\Delta E = 26$ is due to the ungerade $J = 5$ and $J = 7$ states present in the wave packet. The intensities reflect both the excitation probabilities and populations of the states comprising the initial thermal ensemble [14].

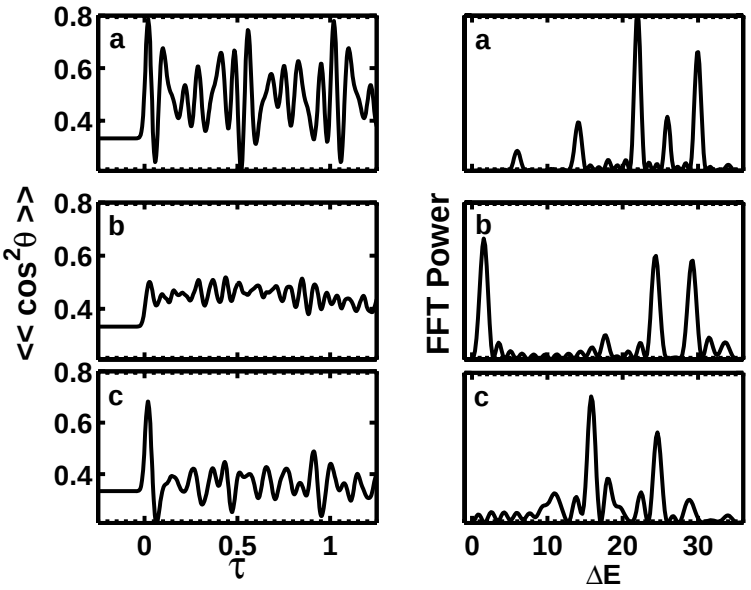

Fig. 1.4. Nonadiabatic alignment by short ($\sigma = 0.032$), intense ($\Delta\omega = 100$) pulses for low temperature ($\gamma = 1$). Time-dependent alignment signals (left panel) and corresponding Fourier transforms (right panel) for a) gas phase, b) cooperative $\langle 100 \rangle$, and c) competitive $\langle 110 \rangle$ polarization of the external field with respect to the internal field ($\kappa = 25$).

Our results for the rotational motion molecules confined in octahedral crystal fields are presented in an analogous way in the middle and lower panel of Fig. 1.4 for the case of of cooperative $\langle 100 \rangle$ and competitive $\langle 110 \rangle$ alignment, respectively. The transient signals $\langle\langle \cos^2 \theta \rangle\rangle(\tau)$ exhibit global maxima near

the center of the pulse. Unexpectedly, the value for the competitive case ($\approx$ 0.7) exceeds that for the cooperative case ($\approx$ 0.5). The further evolution is dominated by post-pulse oscillations for both cases considered here. However, the characteristic revival times found for gas phase molecules are absent and a highly irregular pattern is found instead. Local maxima of 0.5 are found for the cooperative case, while the averaged signal for the competitive case hardly exceeds the isotropic value of 1/3. For a more detailed study of effects of the pulse duration on the transient alignment signals, the interested reader is referred to [14].

A deeper understanding of the field-free evolution has to build on a closer spectral analysis of the post-pulse beating patterns. While wave-packet states of gas phase molecules are composed of free rotor states, the wave-packet states of matrix-isolated molecules can be interpreted as coherent superpositions of librational states. This can be seen from the power spectra of the transient alignment signals in the right panels of Fig. 1.4. The observed frequency patterns correspond to symmetry-allowed transitions between librational, i. e., matrix-induced rotational states. Consequently, all the peaks can be assigned to differences of the energy-levels of the trapped molecule, see Fig. 1.1. While all peaks with $\Delta E > 10$ correspond to transitions between different librational manifolds, the low energy structure found at $\Delta E \approx 1$ is caused by tunnelling transitions within the ground librational manifold. The intensities are governed by the initial populations in the thermal ensemble as well as by rotational excitation probabilities. Since the transition rules and Hönl–London factors for excitations are different within the D_{4h} and D_{2h} point groups, we observe different intensities for the equal frequencies in the cooperative and the competitive cases.

In summary, the analysis of power spectra of experimental nonadiabatic alignment signals lends itself as a novel approach to the analysis of tunnelling and librational energy levels of matrix-isolated molecules. In principle, comparison of experimental data with quantum simulations should, e. g., allow for validation of model potentials such as given in Eq. (1.2) as well as for a determination of the free potential parameters.

As an alternative to the post-pulse alignment created by nonadiabatic alignment, we now turn our attention to the adiabatic case of longer pulses, where alignment is only achieved while the field is on. For gas phase molecules, the adiabatic limit is met if the pulse duration reaches (or exceeds) the rotational period of the molecules under investigation. For matrix-isolated molecules this condition has to be reformulated: Building on the above discussion of tunnelling vs. librational energy scales, it is expected that, for the crystal fields considered here, the pulse lengths have to be one order of magnitude longer in order to reach the adiabatic limit with respect to tunnelling motion. An example can be seen in Fig. 1.5 for various pulse widths σ (FWHM): In all curves ($0.5 \leq \sigma \leq 4$), the maximal alignment, here achieved very close to the center of the pulse, is near the value $\langle\cos^2\theta\rangle_{\max} \to 1 - \sqrt{1/\Delta\omega}$ found for light molecules at low temperatures [53]. However, all curves show also

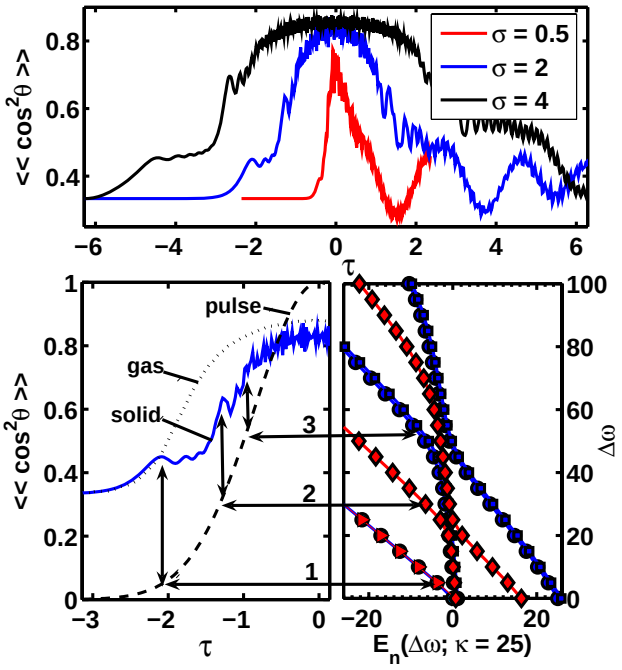

Fig. 1.5. Adiabatic alignment by long, intense ($\Delta\omega = 100$) pulses for low temperature ($\gamma = 1$) and for cooperative $\langle 100 \rangle$ polarization of the external field with respect to the internal field ($\kappa = 25$). Upper: Alignment signal in a time window spanning the whole pulse duration, $-6 \leq \tau \leq 6$. Lower: Stepwise enhancement (enumerated) of alignment signal during onset of the laser pulse (left) together with selected energy levels vs. alignment parameter $\Delta\omega$ (right), see also Fig. 1.2. Reproduced with permission from [14]

a certain degree of oscillatory post-pulse oscillations. For shorter pulses this is similar to the gas phase case, see our previous discussion on nonadiabatic alignment. For the longer pulses the adiabatic limit with respect to librational dynamics has already been reached; however, the oscillations indicate that the pulses are still nonadiabatic with respect to tunnelling dynamics. Indeed, the periods of the field-free oscillations can be exactly assigned to certain tunnelling transitions within the ground librational manifold. In principle these oscillations could be overcome by using even longer pulses. In practice, however, dissipation and de-phasing might become non-negligible on these time scales. Nevertheless we finish this section by stating that adiabatic alignment presents a very promising approach for a highly effective control of rotational degrees of freedom, and can be used to steer the subsequent dynamics, e. g., in subsequent photo-induced processes.

1.6 Conclusions

We have investigated a novel approach to analysis and control of rotational degrees of freedom of linear molecules confined in an octahedral "crystal field" by means of numerical quantum dynamics simulations. The investigated systems serve as simplified models for molecules in rare gas matrices if couplings to translational [38], vibrational [39, 40], or electronic [41] degrees of freedom of the guest molecule are neglected. Building on the well-developed literature for gas phase molecules, alignment and orientation of matrix-isolated molecules induced by laser and static fields has been explored [5, 6, 12–14]. The resulting rotational states can be viewed as hybrids of librational (matrix-induced) or pendular (field-induced) states. If the external control fields are along energetically favored directions of the internal matrix-induced field, cooperative effects are found. Both the degrees of alignment and orientation exceed those obtained in gas phase studies. In general, weak fields are sufficient to align/orient single states, while higher fields are required to achieve the same for thermal ensembles. It is also shown that rotational densities can be controlled at will even though there is competition between internal and external fields, but then higher fields are mandatory. Nevertheless, the examined ranges of interaction strengths can be realized in future applications to demonstrate these effects in rare gas matrix experiments thus opening new approaches to study direction-dependent reaction dynamics of molecules in solids. Typically, such measurements would be performed in the time domain utilizing pulsed light sources where the distinction between nonadiabatic and adiabatic dynamics is based on the ratio of pulse duration and the time scales for tunnelling and librational dynamics of the matrix-isolated molecules. In the nonadiabatic case, ultrashort pulses serve to create non-stationary wavepacket states. The highly oscillating alignment signals in the post-pulse regime can be understood in terms of quantum beats of the comprising librational states. Hence, Fourier transforms of observed, transient alignment signals can be used to analyze the energy level scheme of trapped molecules in a solid which are hard to obtain by continuous infrared spectroscopy [43]. Long pulses close to the adiabatic limit can be used to achieve high degree of alignment during the pulse. Although strictly adiabatic dynamics would have to account for interfering tunnelling states, for the purpose of control it is sufficient to choose pulse widths equal to the rotational period of the free molecule. For both the cooperative and competitive cases studied here, high alignment degrees close to the gas-phase results can be achieved by adiabatic techniques. This allows for preparing suitable precursor states to efficiently control subsequent direction–dependent reaction mechanisms.

References

1. R.B. Gerber, M.V. Korolkov, J. Manz, M.Y. Niv, B. Schmidt, Chem. Phys. Lett. **327**(1–2), 76 (2000)

2. G. Chaban, R.B. Gerber, M.V. Korolkov, J. Manz, M.Y. Niv, B. Schmidt, J. Phys. Chem. A **105**(12), 2770 (2001)
3. B. Schmidt, P. Jungwirth, R.B. Gerber, in *Ultrafast Chemical and Physical Processes in Molecular Systems*, ed. by M. Chergui (World Scientific, Singapore, 1996), pp. 637–640
4. B. Schmidt, P. Jungwirth, Chem. Phys. Lett. **259**(1–2), 62 (1996)
5. T. Kiljunen, M. Bargheer, M. Gühr, N. Schwentner, Phys. Chem. Chem. Phys. **6**(9), 2185 (2004)
6. T. Kiljunen, M. Bargheer, M. Gühr, N. Schwentner, B. Schmidt, Phys. Chem. Chem. Phys. **6**(11), 2932 (2004)
7. J. Manz, P. Saalfrank, B. Schmidt, J. Chem. Soc. Faraday Trans. **93**(5), 957 (1997)
8. P. Jungwirth, Chem. Phys. Lett. **289**(3–4), 324 (1998)
9. P. Jungwirth, P. Ždánská, B. Schmidt, J. Phys. Chem. **102**(37), 7241 (1998)
10. B. Schmidt, Chem. Phys. Lett. **301**(3–4), 207 (1999)
11. P. Ždánská, B. Schmidt, P. Jungwirth, J. Chem. Phys **110**(13), 6246 (1999)
12. T. Kiljunen, B. Schmidt, N. Schwentner, Phys. Rev. Lett. **94**(12), 123003 (2005)
13. T. Kiljunen, B. Schmidt, N. Schwentner, Phys. Rev. A **72**(5), 053415 (2005)
14. T. Kiljunen, B. Schmidt, N. Schwentner, J. Chem. Phys. **124**(16), 164502 (2006)
15. H. Stapelfeldt, T. Seideman, Rev. Mod. Phys. **75**, 543 (2003)
16. B. Friedrich, D. Herschbach, Nature **353**(6343), 412 (1991)
17. H.J. Loesch, Ann. Rev. Phys. Chem. **46**, 555 (1995)
18. B. Friedrich, D. Herschbach, Phys. Rev. Lett. **74**(23), 4623 (1995)
19. B. Friedrich, D. Herschbach, J. Phys. Chem. **99**(42), 15686 (1995)
20. T. Seideman, J. Chem. Phys. **103**(18), 7887 (1995)
21. T. Seideman, J. Chem. Phys. **106**(7), 2881 (1997)
22. J.J. Larsen, K. Hald, N. Bjerre, H. Stapelfeldt, T. Seideman, Phys. Rev. Lett. **85**(12), 2470 (2000)
23. W. Kim, P.M. Felker, J. Chem. Phys. **104**(3), 1147 (1996)
24. W. Kim, P.M. Felker, J. Chem. Phys. **108**(16), 6763 (1998)
25. B. Friedrich, D. Herschbach, J. Chem. Phys. **111**(14), 6157 (1999)
26. B. Friedrich, D. Herschbach, J. Phys. Chem. A **103**(49), 10280 (1999)
27. S. Minemoto, H. Nanjo, H. Tanji, T. Suzuki, H. Sakai, J. Chem. Phys. **118**(9), 4052 (2003)
28. H. Sakai, S. Minemoto, H. Nanjo, H. Tanji, T. Suzuki, Phys. Rev. Lett. **90**(8), 083001 (2003)
29. N.H. Nahler, R. Baumfalk, U. Buck, Z. Bihary, R.B. Gerber, B. Friedrich, J. Chem. Phys. **119**(1), 224 (2003)
30. B. Friedrich, N.H. Nahler, U. Buck, J. Mod. Opt. **50**(15–17), 2677 (2003)
31. T. Seideman, E. Hamilton, Adv. At. Mol. Opt. Phys. **52**, 289 (2005)
32. I.S. Averbukh, R. Arvieu, Phys. Rev. Lett. **87**, 163601 (2001)
33. M. Leibscher, I.S. Averbukh, H. Rabitz, Phys. Rev. Lett. **90**, 213001 (2003)
34. C.Z. Bisgaard, M.D. Poulsen, E. Péronne, S.S. Viftrup, H. Stapelfeldt, Phys. Rev. Lett. **92**, 173004 (2004)
35. P. Marquetand, A. Materny, N.E. Henriksen, V. Engel, J. Chem. Phys. **120**(13), 5871 (2004)
36. J. Ortigoso, Phys. Rev. Lett. **93**(7), 073001 (2004)
37. V.A. Apkarian, N. Schwentner, Chem. Rev. **99**(6), 1481 (1999)
38. H. Friedmann, S. Kimel, J. Chem. Phys. **47**(9), 3589 (1967)

39. S. Hennig, A. Cenian, H. Gabriel, Chem. Phys. Lett. **205**(4–5), 354 (1993)
40. D.M. Villeneuve, S.A. Aseyev, P. Dietrich, M. Spanner, M.Y. Ivanov, P.B. Corkum, Phys. Rev. Lett. **85**(3), 542 (2000)
41. S. Estreicher, T.L. Estle, Phys. Rev. B **30**(1), 7 (1984)
42. J. Manz, J. Am. Chem. Soc. **102**(6), 1801 (1980)
43. V. Berghof, M. Martins, B. Schmidt, N. Schwentner, J. Chem. Phys. **116**(21), 9364 (2002)
44. B. Schmidt, P. Žďánská, Comp. Phys. Comm. **127**(2–3), 290 (2000)
45. A.F. Devonshire, Proc. Roy. Soc. (London) A **153**, 601 (1936)
46. H.U. Beyeler, J. Chem. Phys. **60**(11), 4123 (1974)
47. G.K. Pandey, K.L. Pandey, M. Massey, R. Kumar, Phys. Rev. B **34**(2), 1277 (1986)
48. H. Bethe, Ann. Phys. **3**(2), 132 (1929)
49. L. Pauling, Phys. Rev. **36**, 430 (1930)
50. R.E. Miller, J.C. Decius, J. Chem. Phys. **59**(9), 4871 (1973)
51. J. Ortigoso, M. Rodriguez, M. Gupta, B. Friedrich, J. Chem. Phys. **110**(8), 3870 (1999)
52. F. Rosca-Pruna, M.J.J. Vrakking, J. Chem. Phys. **116**(15), 6567 (2002)
53. T. Seideman, J. Chem. Phys. **115**(13), 5965 (2001)
54. F. Rosca-Pruna, M.J.J. Vrakking, J. Chem. Phys. **116**(15), 6579 (2002)